Spectrochimica Acta Part A: Molecular and Biomolecular Spectroscopy 224 (2020) 117412

Contents lists available at ScienceDirect

Spectrochimica Acta Part A: Molecular and Biomolecular Spectroscopy

journal homepage: www.elsevier.com/locate/saa

Colorimetric assay of acetylcholinesterase inhibitor tacrine based on MoO_2 nanoparticles as peroxidase mimetics

Lingting Huang, Zhihong Li, Liangqia Guo *

Ministry of Education Key Laboratory of Analytical Science of Food Safety and Biology, Fujian Provincial Key Laboratory of Analysis and Detection Technology for Food Safety, College of Chemistry, Fuzhou University, Fuzhou 350116, China

ARTICLE INFO

Article history:
Received 21 April 2019
Received in revised form 19 July 2019
Accepted 20 July 2019
Available online 22 July 2019

Keywords:
MoO_2
Peroxidase mimics
Acetylcholinesterase inhibitor
Colorimetric biosensor

ABSTRACT

Molybdenum dichalcogenides MoX_2 (X = S, Se) have been found to possess intrinsic peroxidase-like activity. However, molybdenum oxides (MoO_2) as peroxidase mimetics have not been exploited yet. Herein, MoO_2 nanoparticles were synthesized by a simple hydrothermal method and found to possess the peroxidase-like activity for the first time. MoO_2 nanoparticles could catalyze the oxidation of 3,3′,5,5′-tetrametylbenzidine (TMB) by H_2O_2 to produce a blue-color product (oxTMB). The catalytic property and mechanism were investigated by stead-state kinetics experiment and free radicals scavenging experiment, respectively. Acetylcholinesterase (AChE) could catalyze the hydrolysis of acetylthiocholine chloride (ATCh) into thiocholine (TCh), which could reduce oxTMB to decrease the absorbance in solution. In the presence of AChE inhibitor tacrine, the generation of TCh was inhibited and the absorbance was preserved. Based on these properties, a colorimetric assay method was developed for AChE inhibitor tacrine. This work not only broadens the application of the peroxidase mimetics, but also overcome the disadvantages of traditional methods such as expensive, complex and vulnerable to background interference for colorimetric assay of AChE inhibitor.

1. Introduction

Alzheimer's disease (AD) is one of the most common neurodegenerative diseases among the elderly people. Acetylcholinesterase (AChE) inhibitors are the cornerstone for the treatment of AD [1]. The inhibitors such as tacrine, donepezil have been approved for the treatment of AD symptom. To search new inhibitors for the development of AD's drug from natural products, a rapid and accurate assay method for AChE inhibitor is necessary. The traditional assay method based on Ellman's reagent is limited by low sensitivity and false-positive effects [2]. There are many alternative methods used to assay AChE inhibitor such as thin layer chromatography (TLC) [3], high performance liquid chromatography-electrospray quadrupole time of flight mass (HPLC-ESI-Q-TOF/MS) [4], electrochemical [5] and fluorescent methods [6–10]. However, these methods require complex operation process or may result in a false-positive effect. Thus, it is highly desired to develop a simple and sensitive assay method for AChE inhibitor.

Since Fe_3O_4 magnetic nanoparticles (NPs) was first reported as peroxidase mimetics in 2007 [11], nanozymes have been attracted wide attention owing to their advantages of high stability, low cost and good catalytic activity as compared with natural enzymes. Today, intrinsic peroxidase activity has been found in many nanomaterials, such as gold NPs [12,13], AgM bimetallic alloy nanostructures (M = Au, Pd, Pt) [14], V_2O_5 nanowires [15], Co_3O_4 NPs [16], $ZnFe_2O_4$ NPs [17], WS_2 nanosheets [18], graphene dots [19], MoS_2 nanosheets [20], graphitic carbon nitrides (g-C_3N_4) [21], graphene oxide [22], metal-organic framework [23,24], $MoSe_2$ nanosheets [25] and so on. Taking advantage of colorimetric method such as simplicity, low cost, and visual observation by naked eyes, peroxidase mimetics have been applied for the colorimetric detection of hydrogen peroxide (H_2O_2) [12,16,19,23,25], glucose [12,16–22,24], ascorbic acid [14,23], xanthine [13,25], organophosphorus pesticides [26] and so on. However, to the best of our knowledge, the application of peroxidase mimetics for colorimetric assay of AChE inhibitor has rarely been studied. Only Prussian blue nanocubes peroxidase mimetic has been reported for colorimetric screening AChE inhibitor using neostigmine as an inhibitor model [27]. The application of peroxidase mimetics-based colorimetric assay of AChE inhibitor is in its infancy.

MoO_2 has been extensively researched in the field of energy storage and considered as a promising anode electrode material for lithium batteries [28]. As transition metal oxides, MoO_2 has similar electrochemical properties with molybdenum dichalcogenides MoX_2 (X = S, Se). It has been reported that both MoS_2 and $MoSe_2$ nanomaterials possessed intrinsic peroxidase-like activity and showed higher affinity to H_2O_2 than HRP [20,25]. For oxygen element belongs to the same main group with sulphur and selenium elements, it is reasonable to infer that MoO_2 nanomaterials may also possess the peroxidase-like activity.

* Corresponding author.
E-mail address: lqguo@fzu.edu.cn (L. Guo).

https://doi.org/10.1016/j.saa.2019.117412
1386-1425/

Nevertheless, peroxidase-like activity of MoO_2 nanomaterials has not been exploited to this day.

Herein, we reported for the first time that MoO_2 NPs possessed an intrinsic peroxidase-like activity and showed a higher affinity to H_2O_2 than $MoSe_2$ nanosheets. The peroxidase substrate 3,3′,5,5′-tetrametylbenzidine (TMB) could be catalytically oxidized into a blue-color product oxTMB to produce obvious color change in the presence of H_2O_2 and MoO_2 NPs. Furthermore, a colorimetric assay of AChE inhibitor was further designed by taking advantage of the peroxidase-like activity of MoO_2 NPs (Scheme 1). Acetylthiocholine chloride (ATCh) was employed as the substrate of AChE. ATCh was catalytically hydrolyzed by AChE into a reducing product thiocholine (TCh) which could reduce oxTMB, resulting in the fading of solution color. It is well-known that many substances such as heavy metals, organophosphorus pesticides, carbamates, etc. can inhibit the activity of AChE in a reversible or irreversible manner [29]. Herein, tacrine, the first drug registered for treatment of AD [30], was used as a model inhibitor of AChE. The inhibitor could inhibit the activity of AChE and retard the fading of solution color. Therefore, a colorimetric assay of AChE inhibitor tacrine based on peroxidase mimetics was proposed for the first time.

2. Experimental section

2.1. Chemicals and materials

H_2O_2 and thiourea were purchased from Sinopharm chemical reagent Co. Ltd. (China). TMB and superoxide dismutase (SOD) were obtained from Shanghai Sangon biological engineering technology and service Co., Ltd. (China). 2,2′-azino-bis(3-ethylbenzothiazoline-6-sulfonicacid) diammonium salt (ABTS) was bought from Bio Basic Inc. (Ontario, Canada). *o*-phenylenediamine (OPD) was bought from Fuzhou DingGuo Biotechnology Co. Ltd. (China). NaN_3 was purchased from Tianjin Fuchen chemical reagents Co. Ltd. (China). Vitamin C (VC) was purchased from Xi'an chemical reagents factory (China). AChE, ATCh, tacrine, and molybdenyl acetylacetonate (MA) were bought from Sigma. Other chemicals were analytical grade. Experimental water was purified by a Millipore Milli-Q purification system with the resistivity 18.2 MΩ·cm.

2.2. Characterization

X-ray diffraction (XRD) pattern was recorded by a powder X-ray diffractometer (Thermo, USA). Transmission electron microscope image was measured by a HT7700 (Hitachi, Japan) transmission electron microscope. X-ray photoelectron spectrum (XPS) was recorded by an ESCALAB 250 X-ray photoelectron spectrometer (VG, USA). The absorption spectrum of solution was recorded by a Lamda 750 UV–vis-NIR spectrometer (PE, USA). Raman spectrum was detected by an inVia Raman spectroscope (Renishaw, UK).

2.3. Preparation of MoO_2 NPs

0.1 g MA was dissolved in the mixed solvent composed of 41 mL water and 9 mL ethanol. After stirring at room temperature for 1 h, the solution was moved to a Teflon-lined stainless steel autoclave and was heated to 180 °C for 20 h. Then, the product was washed for three times with ethanol and water respectively. Finally, the black powder was dried in a vacuum oven at 50 °C. MoO_2 NPs dispersion solution (256 μg mL^{-1}) was prepared by ultrasonic treatment in ultrapure water.

2.4. Colorimetric detection of H_2O_2

For the colorimetric detection of H_2O_2, 200 μL NaAc-HAc buffer (10 mmol L^{-1}, pH 4.0), 50 μL TMB (16 mmol L^{-1}), 50 μL MoO_2 NPs (25.6 μg mL^{-1}) and 200 μL H_2O_2 with different concentration were mixed and incubated at 25 °C in the dark for 40 min, then the absorption spectrum (500–800 nm) of the above mixture solution was recorded.

2.5. Colorimetric assay of AChE inhibitor

100 μL NaAc-HAc (10 mmol L^{-1}, pH 4.0) buffer solution, 100 μL H_2O_2 (400 μmol L^{-1}), 50 μL TMB (16 mmol L^{-1}) and 50 μL MoO_2 NPs (25.6 μg mL^{-1}) were mixed uniformly and the mixture denoted as solution A was incubated at 25 °C in the dark for 20 min.

100 μL tacrine with different concentration and 30 μL AChE (3.5 U mL^{-1}) were evenly mixed in 1.5 mL centrifuge tube and incubated at 25 °C in the dark for 30 min. Then, 20 μL ATCh (10 mmol L^{-1}) and 50 μL NaAc-HAc buffer solution (10 mmol L^{-1}, pH 7.0) were further added into the centrifuge tube. The mixture denoted as solution B was incubated under 25 °C in the dark for another 20 min.

Finally, solution A and B were put together and further incubated at 25 °C in the dark for 30 min. The absorption spectrum (500–800 nm) was recorded.

3. Result and discussion

3.1. Characterization of MoO_2 NPs

MoO_2 NPs were synthesized according to a previous report with a slight modification [31]. The morphology of MoO_2 NPs can be observed by TEM image. As shown in Fig. S1, the as-synthesized MoO_2 NPs are rice-like shape with the size about 10–50 nm. The dispersion solution

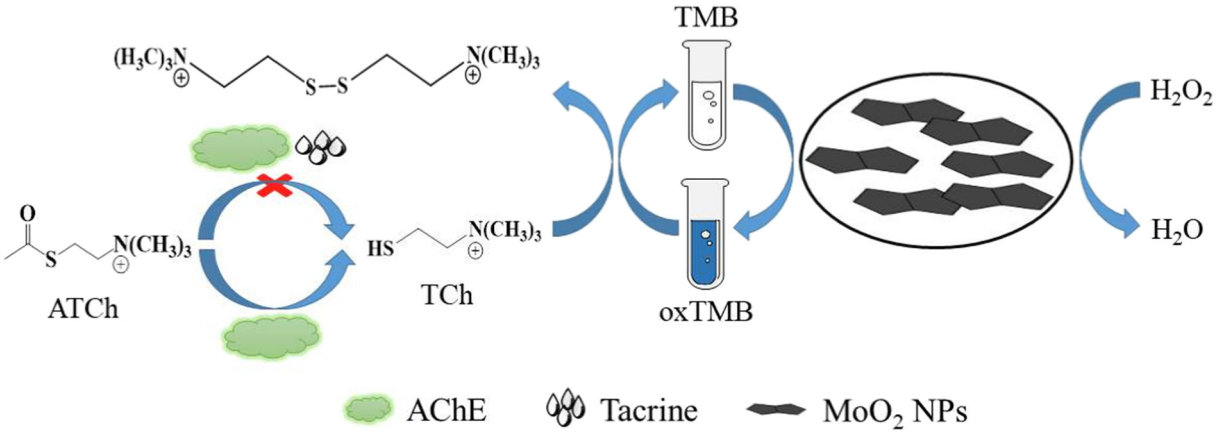

Scheme 1. Schematic illustration of colorimetric assay of AChE inhibitor.

of MoO_2 NPs showed obvious Tyndall effect under the irradiation of a red laser beam (inset of Fig. S1). As shown in Fig. 1A, the XRD pattern indicates that all strong diffraction peaks can be indexed as the monoclinic-phase MoO_2 (JCPDS. 78–1069). Raman spectrum (Fig. 1B) further testifies the monoclinic-phase MoO_2. The peaks of Raman spectra at 662 cm^{-1}, 818 cm^{-1} and 991 cm^{-1} are attributed to the Mo—O bond vibration modes in monoclinic-phase MoO_2. The characteristic peaks at 149 cm^{-1}, 237 cm^{-1}, 283 cm^{-1}, 335 cm^{-1}, 376 cm^{-1} and 456 cm^{-1} can be considered as the phonon vibration [32].

The valence states of Mo atom in MoO_2 NPs were studied by XPS. There are five distinct peaks in the survey spectrum (Fig. 1C), including Mo 3d (230.8 eV), C 1 s (285.2 eV), Mo 3p (396.2 eV and 416.7 eV) and O 1 s (530.6 eV). From the core-level XPS of Mo atom in Fig. 1D, 230.1 eV and 233.4 eV are considered as the peaks of Mo^{4+} $3d_{5/2}$ and Mo^{4+} $3d_{3/2}$, while 231.9 eV and 235.1 eV correspond to Mo^{6+} $3d_{5/2}$ and Mo^{6+} $3d_{3/2}$ [25]. According to the proportion of the peak area of Mo^{4+} and Mo^{6+}, it can be observed that the content of Mo^{4+} is higher that of Mo^{6+} in the MoO_2 NPs sample, indicating that MoO_2 dominates the sample.

3.2. Peroxidase-like activity of MoO_2 NPs

TMB was used as the substrate to investigate the peroxidase-like catalytic activity of MoO_2 NPs. As shown in Fig. 2, the color of TMB solution almost didn't change in the presence of only H_2O_2 or MoO_2 NPs. However, when H_2O_2 and MoO_2 NPs were both added to the TMB solution, the color of the mixture was changed to bright blue with an absorption peak at 652 nm. The similar catalytic oxidation reactions were observed using ABTS and OPD as the HRP substrates (Fig. S2 and S3). These results indicated the peroxidase-like activity of MoO_2 nanoparticles.

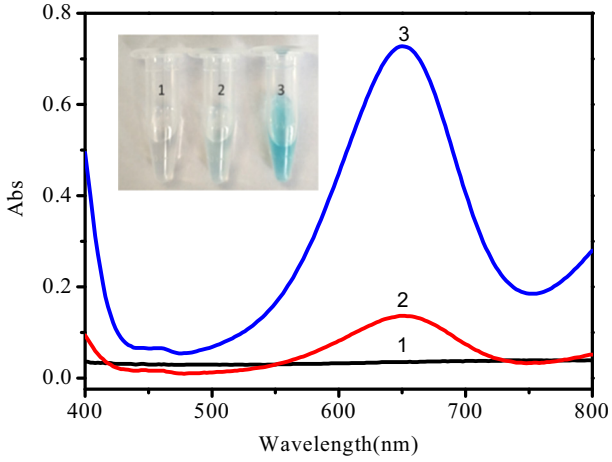

Fig. 2. Absorption spectra of TMB solution in the presence of MoO_2 NPs (1), H_2O_2 (2), MoO_2 NPs and H_2O_2 (3). The inset shows the corresponding photo of the mixture solution. The concentrations of MoO_2 NPs, TMB and H_2O_2 were 2.56 μg mL^{-1}, 1.2 mmol L^{-1}, and 80 μmol L^{-1}, respectively.

3.3. Optimization of reaction conditions

The reaction conditions such as pH, concentration of TMB, reaction temperature, concentration of MoO_2 NPs and reaction time were optimized. MoO_2 NPs showed the highest catalytic activity in pH 4.0 buffer (Fig. S4A), indicating that weak acidic condition is favorable for the catalytic activity of MoO_2 NPs. As shown in Fig. S4B and S4C, the absorption of mixture solution was increased with the increasing concentrations of

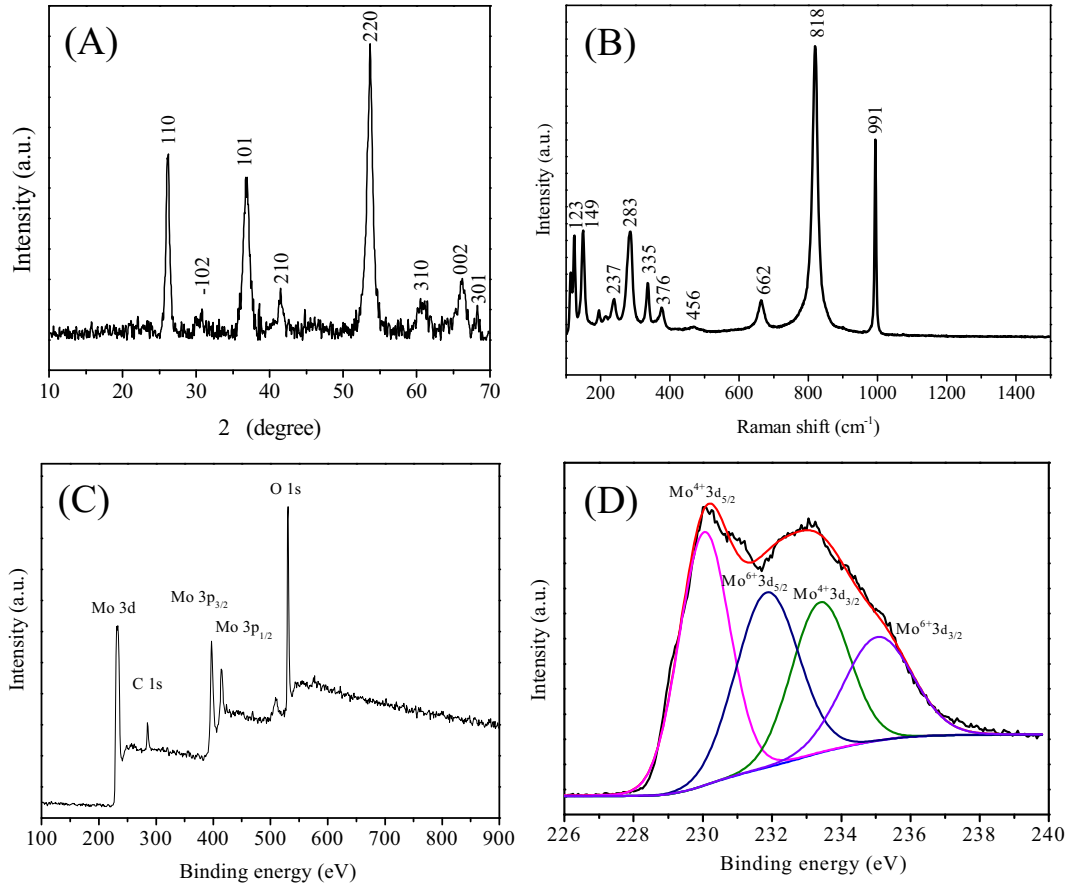

Fig. 1. XRD pattern (A), Raman spectrum (B), XPS survey spectrum (C) and Mo 3d core-level XPS spectrum (D) of as-synthesized MoO_2 NPs.

TMB and MoO_2 NPs and then achieved a platform at 1.6 mmol L^{-1} TMB and 2.56 μg mL^{-1} MoO_2 NPs, respectively. The catalytic activity of MoO_2 NPs was increased with the increasing of temperature from 25 °C to 60 °C and then decreased at higher temperature (Fig. S4D). The absorbance was also increased with the reaction time and almost reached a maximal value at 40 min (Fig. S4E). Therefore, the optimal experiment conditions were chosen as following: pH 4.0, reaction temperature 60 °C, reaction time 40 min and TMB 1.6 mmol L^{-1}, and MoO_2 2.56 μg mL^{-1}. For the simple and convenience of experiment, the room temperature 25 °C was chose for the following experiments.

3.4. Steady-state kinetic parameters

The peroxidase-like catalytic property of MoO_2 NPs was further investigated by steady-state kinetics experiment. The apparent steady-state kinetic parameters were obtained when the concentration of TMB or H_2O_2 was fixed and the concentration of another substrate was changed (Fig. 3A-B). A series of steady-state reaction rates were measured and plotted by using the Lineweaver-Burk plot ($1/v = (K_m/V_{max}) \times (1/[S]) + 1/V_{max}$), where v, K_m, V_{max} and [S] are the initial reaction rate, Michaelis-Menten constant, maximum reaction rate and concentration of substrate, respectively. The K_m and V_{max} values of the catalytic reaction were obtained by the Lineweaver-Burk plot (Fig. 3C-D). As shown in Table 1, the apparent K_m value of MoO_2 NPs was more than 250-fold lower than that of HRP with H_2O_2 as the substrate, implying that the MoO_2 NPs have a higher affinity for H_2O_2 than HRP [11]. Furthermore, similar to MoS_2 nanosheets, MoO_2 NPs also show a higher affinity for H_2O_2 than $MoSe_2$ nanosheets. However, the apparent K_m value with TMB as the substrate was decreased down group 16 chalcogens: $MoO_2 > MoS_2 > MoSe_2$, which indicated an increasing affinity for TMB down group 16 chalcogens. As shown in Fig. 3C-D, the catalytic reaction follows the typical Michaelis-Menten reaction kinetics. The three straight lines were parallel in Fig. 3C-D, which indicated the ping-pong mechanism of the catalytic reaction. Namely, similar to HRP, MoO_2 NPs as the catalyst firstly binds with the first substrate, then generates and releases the first product, and then reacts with the second substrate.

Table 1
Comparison of the kinetic parameters of MoO_2 NPs with MoS_2 nanosheets, $MoSe_2$ nanosheets and HRP.

Catalysts	Substrate	K_m (mmol L^{-1})	V_{max} (mol L^{-1} s^{-1})
MoO_2	H_2O_2	0.0140	0.41×10^{-8}
	TMB	8.85	5.20×10^{-8}
MoS_2 [20]	H_2O_2	0.0116	4.29×10^{-8}
	TMB	0.525	5.16×10^{-8}
$MoSe_2$ [25]	H_2O_2	0.155	0.99×10^{-8}
	TMB	0.014	0.56×10^{-8}
HRP [11]	H_2O_2	3.7	8.71×10^{-8}
	TMB	0.434	10.00×10^{-8}

3.5. Investigation of catalytic mechanism

Various free radical scavenging experiments were designed to further understand the catalytic mechanism of MoO_2 NPs. Free radical scavenger including NaN_3 for $^1O_2$ [20], SOD for $\cdot O_2^-$ [20,33], VC for

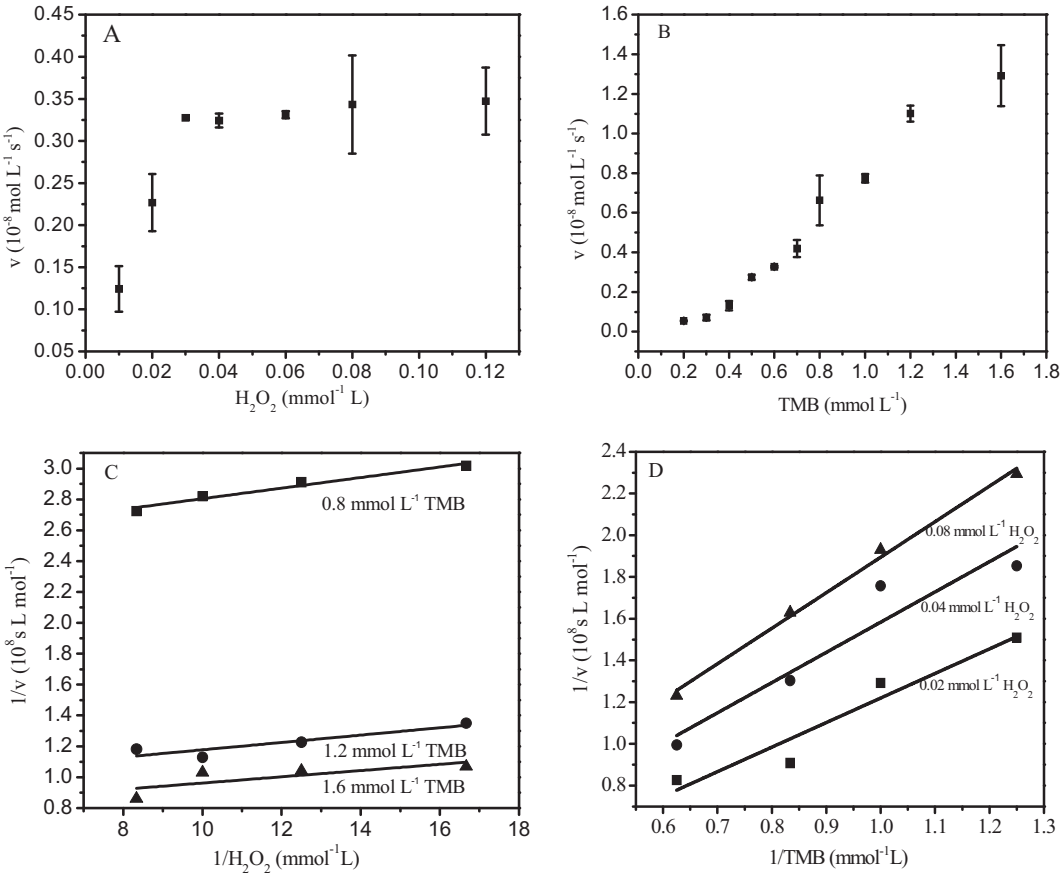

Fig. 3. Steady-state kinetic parameters and catalytic mechanism of MoO_2 NPs (A - D). The catalytic reaction velocity (v) was measured by using MoO_2 NPs (26 μg mL^{-1}) at 25 °C in 0.2 mL NaAc-HAc buffer (10 mmol L^{-1}, pH 4.0). The error bar represents the standard deviation obtained from three repeated measurements. (A) catalytic reaction velocity when TMB concentration was fixed at 0.8 mmol L^{-1} and H_2O_2 concentration was changed; (B) catalytic reaction velocity when H_2O_2 concentration was fixed at 0.02 mmol L^{-1} and TMB concentration was changed; (C, D) Double reciprocal plots of catalytic activity of MoO_2 NPs when the concentration of one substrate (TMB or H_2O_2) is fixed while that of the other is changed.

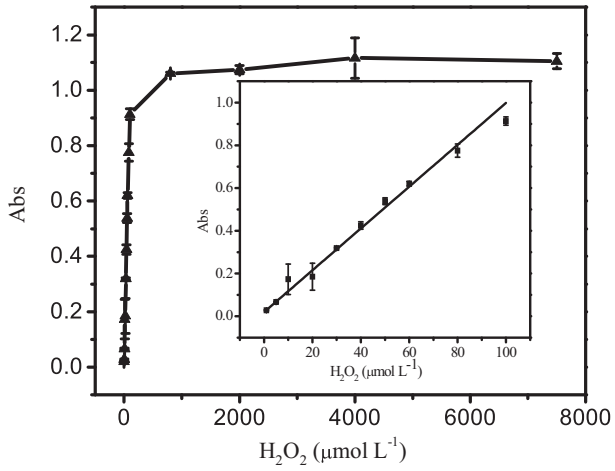

Fig. 4. H_2O_2 concentration-response curve using MoO_2 NPs as peroxidase mimics. The inset shows the calibration plot for H_2O_2. The error bars represent the standard deviation of three measurements.

·OH and $\cdot O_2^-$ [20,33], and thiourea for ·OH [20,33] were used in this experiment. As shown in Fig. S5, when NaN_3 and SOD were added to the reaction system, the absorbance at 652 nm was not decreased, indicating that $^1O_2$ and $\cdot O_2^-$ did not play a key role in the catalytic process. However, the absorbance at 652 nm was decreased significantly on addition of VC and thiourea. These results indicated that the oxidation of TMB was due to ·OH generated from the decomposition of H_2O_2. In addition, the electrochemical performance of MoO_2 nanoparticles was studied by cyclic voltammogram (CV) at different scan rates in a potential range of −0.8 to 0.5 V versus Ag/AgCl (satd. KCl). As shown on Fig. S6, the CV curves possessed good symmetry and no redox peaks were observed. Similar result was observed in previous report [34]. The catalytic MoO_2 nanoparticles are not based on their redox activity. Therefore, it was speculated that MoO_2 NPs could facilitate the electron transfer between H_2O_2 and TMB and accelerate the decomposition of H_2O_2 into ·OH, which oxidized TMB to produce a blue-color product oxTMB.

3.6. Colorimetric detection of H_2O_2

A colorimetric method was designed for the detection of H_2O_2 based on the peroxidase-like activity of MoO_2 NPs. The absorbance at 652 nm was increasing with the concentration of H_2O_2 until H_2O_2 concentration reach 800 μmol L^{-1} (Fig. 4). The linear range for H_2O_2 detection was between 1 μmol L^{-1} and 100 μmol L^{-1} ($R^2 = 0.9965$) (the inset of Fig. 4,) and the detection limit was 0.7 μmol L^{-1} (3σ/k). The sensitivity was comparable to that with MoS_2 nanosheets and $MoSe_2$ nanosheets as peroxidase mimetics.

3.7. Colorimetric assay of AChE inhibitor

Tacrine is one of AChE inhibitors used to treat AD. Based on the inhibition of AChE activity by tacrine, a colorimetric assay of AChE inhibitor was further designed. When AChE and ATCh were added to the MoO_2 NPs-TMB-H_2O_2 solution, AChE catalyzed the hydrolysis of ATCh to produce the reducing product TCh, which reduced the blue-color oxTMB to colorless TMB. However, in the presence of tacrine, the activity of AChE was inhibited, less TCh was produced and the blue-color of solution was preserved. The concentrations of AChE and ATCh were optimized. As shown in Fig. S7 and S8, the absorbance of mixture solution was decreased with the increasing concentrations of AChE and ATCh due to the production of more TCh. Tacking the inhibition efficiency of AChE into account, 3.5 U mL^{-1} AChE and 10 mmol L^{-1} ATCh were chosen for colorimetric assay of AChE inhibitor. As shown in Fig. 5A, the higher the concentration of tacrine added, the higher the absorbance of the solution. Obvious color change could be observed by naked eyes in the presence of 10 nmol L^{-1} of tacrine (Insert of Fig. 5A). The inhibition efficiency (IE) was defined by the following equation: $IE = 100 \times (A_i - A)/(A_0 - A)$, where A_0 was the absorbance (at 652 nm) of the MoO_2 NPs-TMB-H_2O_2 solution in the presence of ATCh, A was the absorbance (at 652 nm) of the MoO_2 NPs-TMB-H_2O_2 solution in the presence of ATCh and AChE. A_i was the absorbance (at 652 nm) of the MoO_2 NPs-TMB-H_2O_2 solution in the presence of ATCh, AChE and inhibitor. As shown in Fig. 5B, the value of IE was increased with the increasing concentration of tacrine. The IE was about 95% in the presence of 200 μmol L^{-1} tacrine. There was a linear relation between IE value and tacrine concentration over the range from 1.0 nmol L^{-1} to 200 nmol L^{-1} ($R^2 = 0.9873$), and the limit of detection was as low as 0.9 nmol L^{-1}. The IC_{50} value, which was the inhibitor concentration needed for 50% inhibition of AChE activity, was calculated to be about 0.32 μmol L^{-1}. This result demonstrated that this method could be utilized for colorimetric assay of AChE inhibitor.

4. Conclusion

In summary, MoO_2 NPs were prepared and found to possess the peroxidase-like activity. Based on the peroxidase-like activity of MoO_2 NPs, a colorimetric method was developed for H_2O_2. Furthermore, a simple, visual and colorimetric assay of AChE inhibitor was designed using tacrine as a model inhibitor. This method provided a sensitive colorimetric detection of tacrine with the limit of detection 0.9 nmol L^{-1}. The color change from colorless to pale blue-color could be

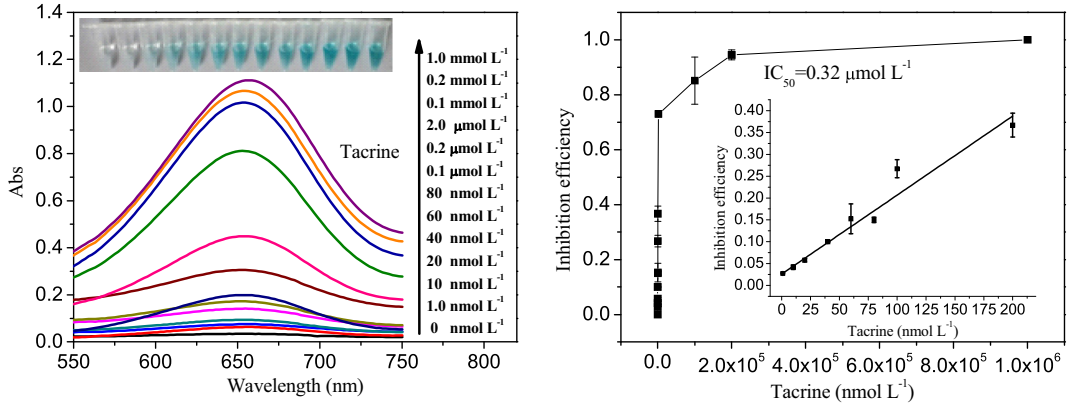

Fig. 5. (A) UV–vis absorption spectra of MoO_2 NPs-TMB-H_2O_2 solution on addition of 0.4 mmol L^{-1} ATCh, 210 mU mL^{-1} AChE and various concentrations of tacine. (B) Plot of IE of tacine toward AChE versus the concentration of tacrine. Insert of (A) showed the color of corresponding solution. The concentrations of tacine (from left to right) are 0, 1, 10, 20, 40, 60, 80, 100, 200, 2000, 100,000, 200,000, 1,000,000 (nmol L^{-1}), respectively. Insert of (B) showed the calibration curve for tacrine.

discriminated by naked eyes in the presence of as low as 10 nmol L^{-1} of tacrine. The IC_{50} value of tacrine for AChE was about 0.32 μmol L^{-1}. It is expected that this method can be used for the measurement of AChE activity and preliminary screening of AChE inhibitors to discover new drugs for AD curing.

Acknowledgements

This work was financially supported by the National Natural Science Foundation of China (21577017), the Science and Technology Project of Fujian Province of China (2017Y0057) and the Program for Changjiang Scholars and Innovative Research Team in University of Ministry of Education of China (IRT15R11).

Appendix A. Supplementary data

Supplementary data to this article can be found online at https://doi.org/10.1016/j.saa.2019.117412.

References

[1] H. Dvir, I. Silman, M. Harel, T.L. Rosenberry, J.L. Sussman, Acetylcholinesterase: from 3D structure to function, Chem. Biol. Interact. 187 (2010) 10–22.
[2] M. Wang, X. Gu, G. Zhang, D. Zhang, D. Zhu, Continuous colorimetric assay for acetylcholinesterase and inhibitor screening with gold nanoparticles, Langmuir 25 (2009) 2504–2507.
[3] I.A. Ramallo, M.O. Salazar, R.L.E. Furlan, Thin layer chromatography-autography-high resolution mass spectrometry analysis: accelerating the identification of acetylcholinesterase inhibitors, Phytochem. Anal. 26 (2015) 404–412.
[4] H. Zhao, S. Zhou, M. Zhang, J. Feng, S. Wang, D. Wang, Y. Geng, X. Wang, An in vitro AChE inhibition assay combined with UF-HPLC-ESI-Q-TOF/MS approach for screening and characterizing of AChE inhibitors from roots of *Coptis chinensis Franch*, J. Pharm. Biomed. Anal. 120 (2016) 235–240.
[5] Y. Tian, S. Ye, X. Shi, L. Jing, C. Liang, Y. Xian, An electrochemical platform for acetylcholinesterase activity assay and inhibitors screening based on Michael addition reaction between thiocholine and catechol-terminated SAMs, Analyst 136 (2011) 5084–5090.
[6] F. Feng, Y. Tang, S. Wang, Y. Li, D. Zhu, Continuous fluorometric assays for acetylcholinesterase activity and inhibition with conjugated polyelectrolytes, Angew. Chem. Int. Ed. 46 (2007) 7882–7886.
[7] J. Chen, D. Liao, Y. Wang, H. Zhou, W. Li, C. Yu, Real-time fluorometric assay for acetylcholinesterase activity and inhibitor screening through the pyrene probe monomer-excimer transition, Org. Lett. 15 (2013) 2132–2135.
[8] P. Ni, Y. Sun, S. Jiang, W. Lu, Y. Wang, Z. Li, Z. Li, Label-free detection of acetylcholinesterase and its inhibitor based on the in situ formation of fluorescent copper nanoparticles, Sensors Actuators B Chem. 240 (2017) 651–656.
[9] R.-L. Zhang, S.-S. Liang, M. Jin, T. He, Z.-Q. Zhang, Simple and sensitive fluorescence assay for acetylcholinesterase activity detection and inhibitor screening based on glutathione-capped gold nanoclusters, Sensors Actuators B Chem. 253 (2017) 196–202.
[10] J. Xu, F. Zhou, L. Chen, G. Chen, S. Pan, Z. Qian, H. Feng, Thiol-triggered disaggregation-induced emission controlled by competitive coordination for acetylcholinesterase monitoring and inhibitor screening, Sensors Actuators B Chem. 255 (2018) 22–28.
[11] L. Gao, J. Zhuang, L. Nie, J. Zhang, Y. Zhang, N. Gu, T. Wang, J. Feng, D. Yang, S. Perrett, X. Yan, Intrinsic peroxidase-like activity of ferromagnetic nanoparticles, Nat. Nanotechnol. 2 (2007) 577–583.
[12] Y. Jv, B. Li, R. Cao, Positively-charged gold nanoparticles as peroxidase mimic and their application in hydrogen peroxide and glucose detection, Chem. Commun. 46 (2010) 8017–8019.
[13] X.-X. Wang, Q. Wu, Z. Shan, Q.-M. Huang, BSA-stabilized Au clusters as peroxidase mimetics for use in xanthine detection, Biosens. Bioelectron. 26 (2011) 3614–3619.
[14] W. He, X. Wu, J. Liu, X. Hu, K. Zhang, S. Hou, W. Zhou, S. Xie, Design of AgM bimetallic alloy nanostructures (M=Au, Pd, Pt) with tunable morphology and peroxidase-like activity, Chem. Mater. 22 (2010) 2988–2994.
[15] R. André, F. Natálio, M. Humanes, J. Leppin, K. Heinze, R. Wever, H.-C. Schröder, W.E.G. Müller, W. Tremel, V_2O_5 nanowires with an intrinsic peroxidase-like activity, Adv. Funct. Mater. 21 (2011) 501–509.
[16] J. Mu, Y. Wang, M. Zhao, L. Zhang, Intrinsic peroxidase-like activity and catalase-like activity of Co_3O_4 nanoparticles, Chem. Commun. 48 (2012) 2540–2542.
[17] L. Su, J. Feng, X. Zhou, C. Ren, H. Li, X. Chen, Colorimetric detection of urine glucose based $ZnFe_2O_4$ magnetic nanoparticles, Anal. Chem. 84 (2012) 5753–5758.
[18] T. Lin, L. Zhong, Z. Song, L. Guo, H. Wu, Q. Guo, Y. Chen, F. Fu, G. Chen, Visual detection of blood glucose based on peroxidase-like activity of WS2 nanosheets, Biosens. Bioelectron. 62 (2014) 302–307.
[19] A.-X. Zheng, Z.-X. Cong, J.-R. Wang, J. Li, H.-H. Yang, G.-N. Chen, Highly-efficient peroxidase-like catalytic activity of graphene dots for biosensing, Biosens. Bioelectron. 49 (2013) 519–524.
[20] T. Lin, L. Zhong, L. Guo, F. Fu, G. Chen, Seeing diabetes: visual detection of glucose based on the intrinsic peroxidase-like activity of MoS_2 nanosheets, Nanoscale 6 (2014) 11856–11862.
[21] T. Lin, L. Zhong, J. Wang, L. Guo, H. Wu, Q. Guo, F. Fu, G. Chen, Graphite-like carbon nitrides as peroxidase mimetics and their applications to glucose detection, Biosens. Bioelectron. 59 (2014) 89–93.
[22] Y. Song, K. Qu, C. Zhao, J. Ren, X. Qu, Graphene oxide: intrinsic peroxidase catalytic activity and its application to glucose detection, Adv. Mater. 22 (2010) 2206–2210.
[23] J.-W. Zhang, H.-T. Zhang, Z.-Y. Du, X. Wang, S.-H. Yu, H.-L. Jiang, Water-stable metal-organic frameworks with intrinsic peroxidase-like catalytic activity as a colorimetric biosensing platform, Chem. Commun. 50 (2014) 1092–1094.
[24] Y. Huang, M. Zhao, S. Han, Z. Lai, J. Yang, C. Tan, Q. Ma, Q. Lu, J. Chen, X. Zhang, Z. Zhang, B. Li, B. Chen, Y. Zong, H. Zhang, Growth of Au nanoparticles on 2D metalloporphyrinic metal-organic framework nanosheets used as biomimetic catalysts for cascade reactions, Adv. Mater. 29 (2017), 1700102.
[25] X. Wu, T. Chen, J. Wang, G. Yang, Few-layered $MoSe_2$ nanosheets as an efficient peroxidase nanozyme for highly sensitive colorimetric detection of H_2O_2 and xanthine, J. Mater. Chem. B 6 (2018) 105–111.
[26] M. Liang, K. Fan, Y. Pan, H. Jiang, F. Wang, D. Yang, D. Lu, J. Feng, J. Zhao, L. Yang, X. Yan, Fe_3O_4 magnetic nanoparticle peroxidase mimetic-based colorimetric assay for the rapid detection of organophosphorus pesticide and nerve agent, Anal. Chem. 85 (2013) 308–312.
[27] P. Ni, Y. Sun, H. Dai, W. Lu, S. Jiang, Y. Wang, Z. Li, Z. Li, Prussian blue nanocubes peroxidase mimetic-based colorimetric assay for screening acetylcholinesterase activity and its inhibitor, Sensors Actuators B Chem. 240 (2017) 1314–1320.
[28] B. Guo, X. Fang, B. Li, Y. Shi, C. Ouyang, Y.-S. Hu, Z. Wang, G.D. Stucky, L. Chen, Synthesis and lithium storage mechanism of ultrafine MoO_2 nanorods, Chem. Mater. 24 (2012) 457–463.
[29] Y. Miao, N. He, J.-J. Zhu, History and new developments of assays for cholinesterase activity and inhibition, Chem. Rev. 110 (2010) 5216–5234.
[30] E. Giacobini, Cholinesterase inhibitors for Alzheimer's disease therapy: from tacrine to future applications, Neurochem. Int. 32 (1998) 413–419.
[31] Q. Zhang, X. Li, Q. Ma, Q. Zhang, H. Bai, W. Yi, J. Liu, J. Han, G. Xi, A metallic molybdenum dioxide with high stability for surface enhanced Raman spectroscopy, Nat. Commun. 8 (2017), 14903.
[32] Q. Zhang, X. Li, W. Yi, W. Li, H. Bai, J. Liu, G. Xi, Plasmonic MoO_2 nanospheres as a highly sensitive and stable non-noble metal substrate for multicomponent surface-enhanced Raman analysis, Anal. Chem. 89 (2017) 11765–11771.
[33] Y. Tang, Y. Su, N. Yang, L. Zhang, Y. Lv, Carbon nitride quantum dots: a novel chemiluminescence system for selective detection of free chlorine in water, Anal. Chem. 86 (2014) 4528–4535.
[34] E. Zhou, C. Wang, Q. Zhao, Z. Li, M. Shao, X. Deng, X. Liu, X. Xu, Facile synthesis of MoO_2 nanoparticles as high performance supercapacitor electrodes and photocatalysts, Ceram. Int. 42 (2016) 2198–2203.